Article

Recent global climate feedback controlled by Southern Ocean cooling

Sarah M. Kang [1] ✉, **Paulo Ceppi** [2] ✉, **Yue Yu** [3] **& In-Sik Kang** [3]

The magnitude of global warming is controlled by climate feedbacks associated with various aspects of the climate system, such as clouds. The global climate feedback is the net effect of these feedbacks, and its temporal evolution is thought to depend on the tropical Pacific sea surface temperature pattern. However, current coupled climate models fail to simulate the pattern observed in the Pacific between 1979 and 2013 and its associated anomalously negative feedback. Here we demonstrate a mechanism whereby the Southern Ocean controls the global climate feedback. Using climate model experiments in which Southern Ocean sea surface temperatures are restored to observations, we show that accounting for recent Southern Ocean cooling—which is absent in coupled climate models—halves the bias in the global climate feedback by removing the cloud component bias. This global impact is mediated by a teleconnection to the Southeast Pacific, where remote sea surface temperature anomalies cause a strong stratocumulus cloud feedback. We propose that this Southern Ocean-driven pattern effect is underestimated in most climate models, owing to an overly weak stratocumulus cloud feedback. Addressing this bias may shift climate sensitivities to higher values than currently simulated as the Southern Ocean undergoes accelerated warming in future projections.

How much Earth will warm in the future is a pressing question in climate science. The rate of global surface warming in response to a radiative forcing is determined by climate feedback processes such as those associated with changes in clouds, sea ice and water vapour[1]. Net climate feedback is negative as the climate system acts to counteract the forcing; otherwise, the system would be unstable. Over the last decade, research has identified that the magnitude of climate feedback is not constant because of its dependence on the spatial structure of sea surface temperature (SST) change—a phenomenon known as the 'pattern effect'[2].

As evolving SST patterns are recognized as being essential to the temporally varying climate feedback, a number of studies have adopted a Green's function approach to identify the SST change pattern that is responsible for causing changes in global climate feedback[3,4].

Surface warming in ascent regions of the western tropical Pacific has been found to play a dominant role, consistent with observational evidence[5]. Warming in the western Pacific ascent region effectively warms free-tropospheric air throughout the tropics, thereby increasing the lower-tropospheric stability, which then acts to increase low cloud cover over remote subsidence regions such as the East Pacific, enhancing the reflection of solar radiation[6]. A stronger zonal SST gradient in the tropical Pacific therefore yields a more negative climate feedback and vice versa. Hence, the climate feedback becomes less negative with time after an abrupt increase in radiative forcing as the eastern tropical Pacific warming gradually intensifies[7].

By contrast, in atmosphere-only climate model simulations of the recent past since 1979 forced with observed SSTs, climate feedback is substantially more negative than in the long-term mean due

[1]Max Planck Institute for Meteorology, Hamburg, Germany. [2]Department of Physics, Imperial College London, London, UK. [3]State Key Laboratory of Satellite Ocean Environment Dynamics, Second Institute of Oceanography, Ministry of Natural Resources, Hangzhou, China. ✉e-mail: sarah.kang@mpimet.mpg.de; p.ceppi@imperial.ac.uk
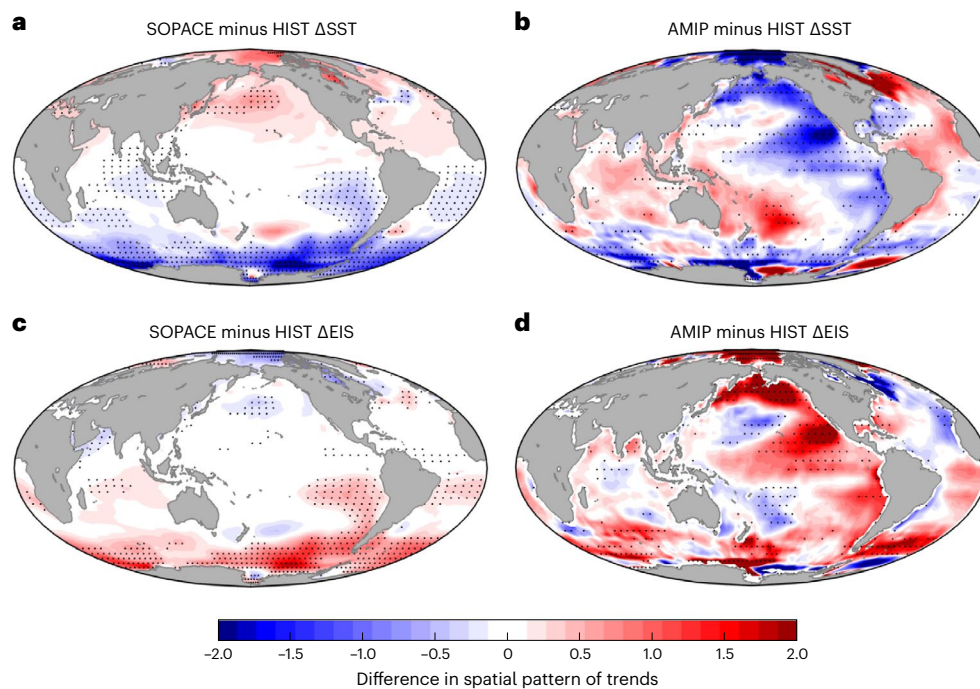
Fig. 1 | Differences in the spatial pattern of SST and estimated inversion strength trends. The pattern of change is calculated by regressing local annual-mean SST (or EIS) against global-mean annual-mean surface air temperature. **a,b**, Differences in the spatial pattern of SST trends between SOPACE and HIST (**a**) and AMIP and HIST (**b**). **c,d**, Similar to **a,b**, but for EIS. Regions with a pattern difference significant at the 95% confidence level based on a Student's *t* test are stippled.

to a prominent cooling in the eastern tropical Pacific[8–12]. This recent trend is notoriously not captured by coupled global climate models under historical forcing because of a robust bias in the observed and simulated SST trend patterns[8,13] (Extended Data Fig. 1), particularly in terms of the so-called La Niña-like cooling in the East Pacific. However, the SST trends also differ noticeably in the Southern Ocean, where the observed prominent cooling is missing in models. Observed cooling trends in the Southern Ocean and the tropical Pacific have been suggested to be related, with the latter driving the former as part of the Interdecadal Pacific Oscillation[14,15]. On the other hand, the Southern Ocean cooling may have instead arisen independent of the tropical Pacific cooling: being internally generated through changes in deep water formation[16] and/or forced by increased Antarctic freshwater fluxes[17–19] and stratospheric ozone depletion[20,21]. Regardless of the cause, the Southern Ocean cooling itself was recently revealed to have the capacity to affect the southern subtropics and their extensive stratocumulus cloud decks[22–25], thereby potentially modifying the global radiative budget. Hence, we hypothesize that the Southern Ocean cooling may have contributed to the anomalously negative climate feedback in the recent historical period. A similar hypothesis was recently proposed based on observed statistical relationships between the Southern Annular Mode and the SSTs in the South Pacific[26], but this study mechanistically demonstrates and quantifies the impact of the observed Southern Ocean cooling on the global energy budget.

While the role of the tropical Pacific zonal SST gradient has been highlighted in the context of the pattern effect[3,4,6,8,9,27,28], here we identify the Southern Ocean SST trend as an important determinant of global climate feedback through the teleconnection to the Southeast Pacific. The Southern Ocean has previously been shown to contribute to more positive global feedbacks on centennial timescales through cloud feedback and ocean heat release[29–31]. This local perspective should be distinguished from our proposed Southern Ocean-driven pattern effect, which emphasizes the remote influence on the southeastern tropical Pacific.

Assessing the remote impacts of Southern Ocean cooling

Our focus is on the period 1979–2013 when the Southern Ocean surface cooled substantially in observations, but the climate model simulations under historical forcings are dominated by the global warming tendency (Extended Data Fig. 1). This contrast can be confirmed from the difference in the SST trend pattern for Atmospheric Model Intercomparison Project (AMIP), with prescribed observed historical SST and radiative forcings, and the coupled historical (HIST) simulations, both of which are conducted with Community Earth System Model 2 (CESM2)[32] (Fig. 1b). To isolate the role of observed Southern Ocean cooling on global climate feedback, we conduct a Southern Ocean Pacemaker (SOPACE) experiment[33] with CESM2, where SST anomalies poleward of 40° S are nudged towards the observed evolution (Methods and Extended Data Table 1). Here we define the Southern Ocean as poleward of 40° S, which corresponds to the region with cooling trends in the observations (Extended Data Fig. 1d). In addition to the imposed Southern Ocean cooling in SOPACE, a clear cooling signal extends equatorward into the Southeast Pacific (Fig. 1a). A recent study shows that this Southern Ocean-driven teleconnection is modulated by Southeast Pacific cloud changes[25]. Hence, CESM2 is an ideal choice for the present study because it simulates a realistically strong increase in Southeast Pacific cloud fraction in the recent past (Extended Data Fig. 2), and correspondingly, its low-cloud feedback is also close to observations (Fig. 2 and Extended Data Figs. 3 and 4). Most other Coupled Model Intercomparison Project Phase 6 (CMIP6) models severely underestimate this cloud response. Note that the Southeast Pacific feedback is negative relative to global-mean temperature but positive relative to the local SST. Methods provide more details about the sensitivity to the choice of model (Extended Data Fig. 5). The equatorward teleconnection is preferentially through the eastern basin owing to climatological southeasterlies and is further amplified by wind–evaporation–SST feedback, Ekman-induced coastal upwelling and cloud radiative feedback[25].
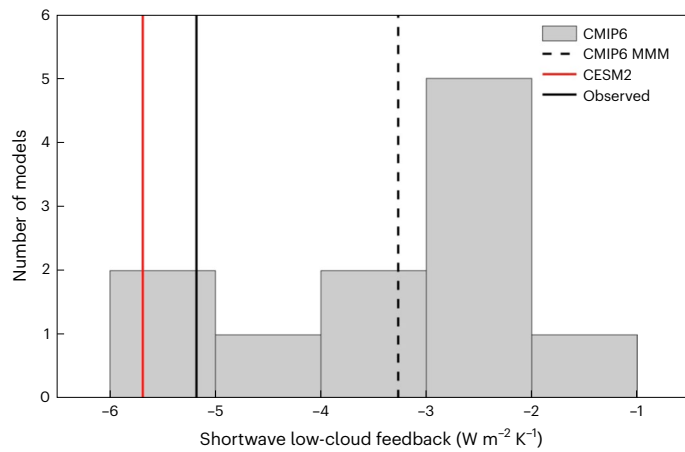
Fig. 2 | Southeast Pacific-averaged shortwave radiative feedbacks. Histogram of shortwave low-cloud radiative feedbacks $\lambda_{swcld,low}$ predicted via cloud-controlling-factor analysis (Methods) averaged over the Southeast Pacific (a trapezoidal area in Fig. 3) from 11 CMIP6 models, with the multi-model mean (MMM) as a black dashed line. The black solid line indicates the observed estimate inferred from MODIS observations, and the red solid line indicates the CESM2 value.

The difference in SST trend pattern gives rise to the difference in the spatial pattern of trends in estimated inversion strength (EIS), a measure of the effective stability of the lower troposphere and a key control of marine low-cloud amount[34]. The spatial patterns of SST and EIS are strongly anti-correlated at −0.92 for the difference between SOPACE and HIST (Fig. 1a,c). This is consistent with the SST pattern being the main control of the tropospheric stability[27], particularly in the tropics where free-tropospheric temperatures are set by the SST over warm convective regions[35]. Hence, the EIS increases if local SST increases less than in the warm pool; conversely, the EIS decreases if local SST increases more, establishing a strong anti-correlated

relationship between EIS and the relative SST. It is noteworthy that the correspondence between the SST and EIS trend patterns also applies to extratropically driven climate change. This is because the extratropics-to-tropics teleconnection takes place primarily through changes in SST[36,37], and hence, the Southern Ocean cooling leads to EIS increasing both locally and remotely in the southeastern tropical Pacific.

As the Southern Ocean SST trends are forced to follow observations in SOPACE, the spatial patterns of SST and EIS trends closely match those in AMIP south of the equator (Fig. 1). While substantial differences remain between SOPACE and AMIP in the North Pacific and Indian oceans, possibly associated with the Pacific Decadal Oscillation[38], we emphasize that our aim is not to reproduce the observed climate change pattern in its entirety but rather to assess the potential effect of observed Southern Ocean cooling in isolation. Because decreasing SST and increasing EIS both imply enhanced marine low cloud cover[27,34], SOPACE exhibits a more negative cloud feedback relative to HIST over the southern extratropics and southeastern tropical Pacific (Fig. 3a). These radiative changes in the Southeast Pacific reflect an increasing trend of total cloud amount, consistent with satellite observations (Extended Data Fig. 2). Although the SST nudging is restricted to the Southern Ocean, the cloud feedback change averaged over the southeastern tropical Pacific outweighs that averaged poleward of 40° S by a factor of 5.66 (Fig. 3c). This is because the Southeast Pacific is characterized by a strong stratocumulus cloud feedback in CESM2[25] (Fig. 2), broadly consistent with observations[39,40] and acting to amplify the local negative SST anomalies, despite differences in the details of the spatial distribution (Extended Data Figs. 3, 4 and 6). Despite the small areal coverage of 3.4% of the global surface, the southeastern tropical Pacific contributes to 25.8% of the global cloud feedback difference between SOPACE and HIST (Fig. 3d). This change in cloud feedback almost entirely explains the change in total radiative feedback (Fig. 3a,e), demonstrating the effectiveness of the Southern Ocean in modulating the global climate feedback through remote cloud changes off the west coast of South America.
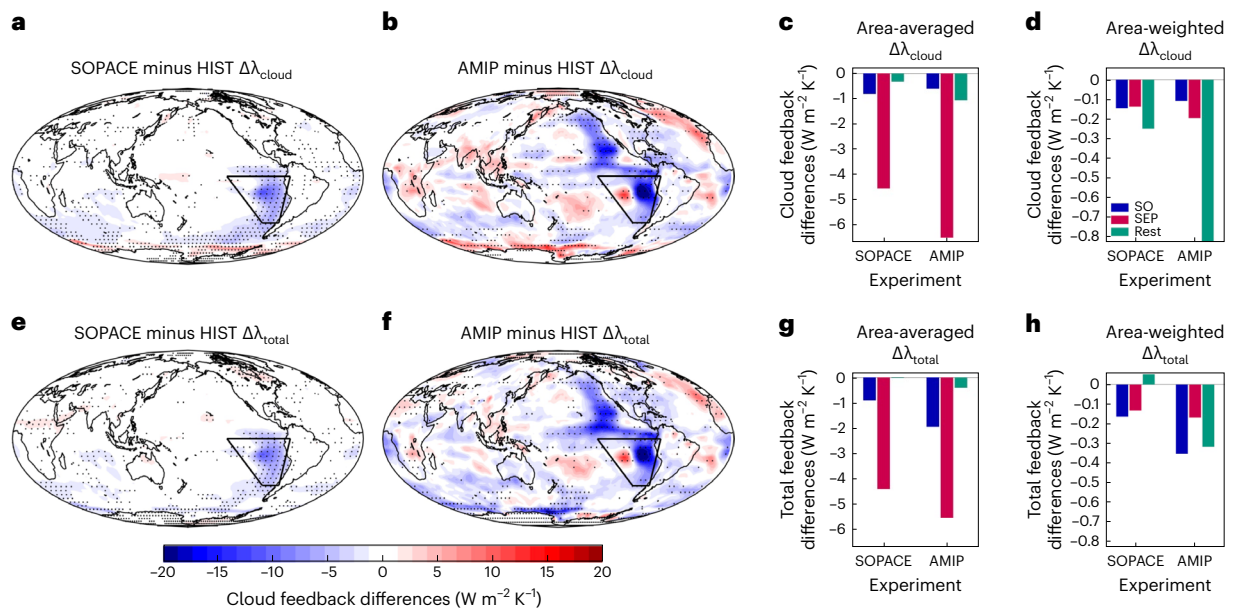
Fig. 3 | Differences in the spatial patterns of climate feedbacks and regional contributions. a,b, Cloud feedback λ_{cloud} differences between SOPACE and HIST (**a**) and AMIP and HIST (**b**). Regions with the difference significant at the 95% confidence level based on a Student's *t* test are stippled. **c,** λ_{cloud} differences averaged over the Southern Ocean (poleward of 40° S; blue), the Southeast Pacific (denoted by black contours; red) and the rest of the globe (green).

d, Area-averaged λ_{cloud} differences multiplied by the fractional area (that is, 18% for the Southern Ocean, 3% for the Southeast Pacific and 79% for the rest of the globe). **e–h,** Similar to **a–d**, but for the total climate feedback λ_{total}. Black contours indicate the Southeast Pacific, defined as a trapezoid based on the following coordinates: (140° W, 0°), (75° W, 0°), (70° W, 40° S), (90° W, 40° S). Note that λ_{cloud} and λ_{total} in HIST are provided in Extended Data Fig. 6.
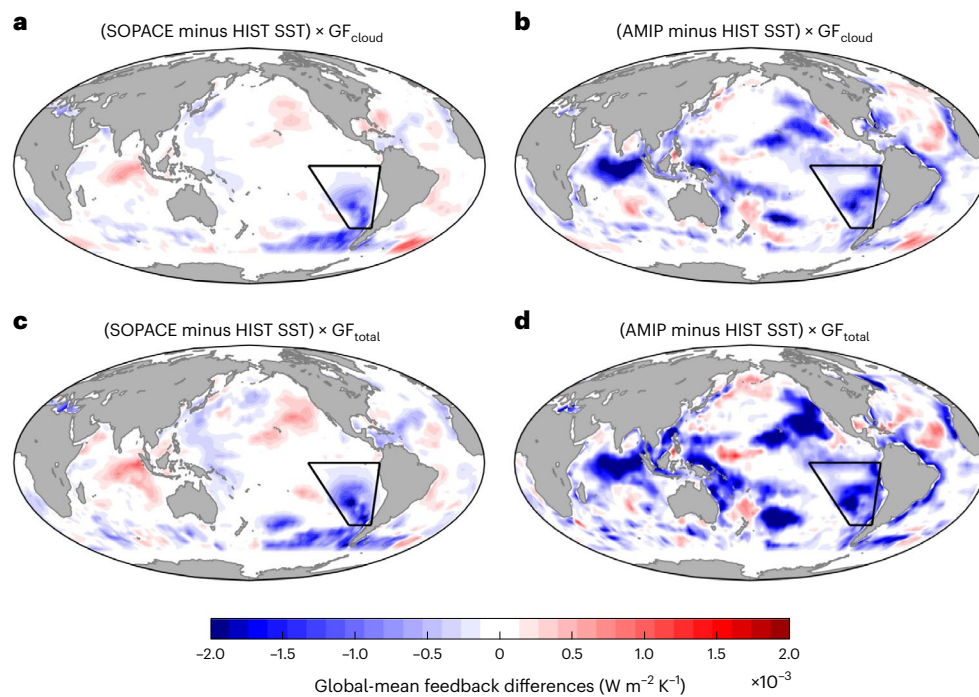
Fig. 4 | Contributions of local SST pattern differences to global-mean climate feedback differences Δλ. a, Green's function for cloud feedback multiplied by the difference in SST pattern changes between SOPACE and HIST (**a**) and AMIP and HIST (**b**). **c**,**d**, Similar to **a** and **b**, but for total climate feedback. The Green's function maps are shown in Extended Data Fig. 7. Global sum corresponds to the global-mean climate feedback difference Δλ.

The spatial patterns of cloud and total feedback in SOPACE are similar to those of the Southern Hemisphere in AMIP (Fig. 3a,e versus 3b,f). As in SOPACE, the southeastern tropical Pacific dominates the area-averaged cloud and total feedback changes in AMIP (Fig. 3c,g). In fractional terms, the southeastern tropical Pacific contributes to global cloud and total feedback differences between AMIP and HIST by 17.3% and 20.0%, respectively (Fig. 3d,h). This suggests a critical role of the southeastern tropical Pacific cooling for the anomalously negative decadal climate feedback during 1979–2013. Our SOPACE experiment further indicates that the southeastern tropical Pacific cooling may have been in large part driven by the Southern Ocean cooling. Whereas one may raise the possibility of the Southeast Pacific cooling and, in turn, the Southern Ocean cooling being driven by the tropical Pacific, in reality, we note that the Southeast Pacific has been found to be more responsive to the Southern Ocean than to the tropical Pacific[33].

Regional contributions to global feedback changes

To quantify the relative contributions of regional SST changes to the global feedback changes, we adopt the Green's function approach[3,4] (Methods). Multiplying the Green's function by the SST difference patterns (Fig. 4) allows us to attribute the global feedback changes to regional SST changes. The Southeast Pacific stands out in SOPACE as a key contribution to the global radiative feedback changes (Fig. 4a,c). In contrast to the notion of the western Pacific ascent region exerting a dominant control on global radiative feedback changes[3], as indicated by the Green's function (Extended Data Fig. 7), this region contributes little in our SOPACE experiment. In AMIP, many different regions contribute to the negative global feedback, including not only the warm-pool region but also the Northeast Pacific, the South Pacific Convergence Zone and the Southeast Pacific (Fig. 4b,d). The strong response of Southeast Pacific SST to Southern Ocean cooling, demonstrated by SOPACE, suggests that the Southeast Pacific contribution to the global radiative feedback changes in AMIP is induced by the Southern Ocean.

Correspondingly, accounting for the Southern Ocean cooling in the historical period shifts the global cloud and total radiative feedbacks towards more negative values from those in the historical simulations (contrast the red circles and green crosses in Fig. 5). That is, the discrepancy in the global feedbacks between HIST and AMIP simulations can be partly attributed to the inability of the coupled simulations under historical forcings to simulate the observed Southern Ocean cooling. The differences in global cloud and total radiative feedback changes from the historical simulations for both SOPACE and AMIP are adequately reconstructed using Green's function, which validates the utility of the Green's function approach (contrast 'CESM2' with 'CESM2 reconstructed' in Fig. 5).

Shifting away from the prevailing paradigm whereby the West Pacific warm pool alone determines the time evolution of global climate feedback[3,4,6,8,9,27,28], our results reveal a novel mechanism by which the Southern Ocean controls global climate feedback via remote changes in SST and lower-tropospheric stability. Most attention has been paid to the western Pacific warm-pool region because of its ability to exert a non-local effect on the extensive marine low-cloud decks of the East Pacific, as revealed by Green's function (Extended Data Fig. 7). Compared to the warm pool, the Southern Ocean does not stand out as an important contribution to the global radiative feedback, according to Green's function. However, when the remote Southeast Pacific SST changes are included, the actual contribution of the Southern Ocean is, in fact, substantial. For instance, the bias in global total radiative feedback λ in the CESM2 historical simulation is approximately halved when the observed historical pattern of Southern Ocean cooling is accounted for in SOPACE (Fig. 5b). The Southern Ocean-driven pattern effect is not represented by the Green's function because the teleconnection is mediated through remote changes in SST, while Green's function is constructed with fixed-SST simulations that do not allow for remote responses. This, hence, highlights the critical limitation of the Green's function approach for a quantitative attribution of the importance of different regions for the global radiation budget.
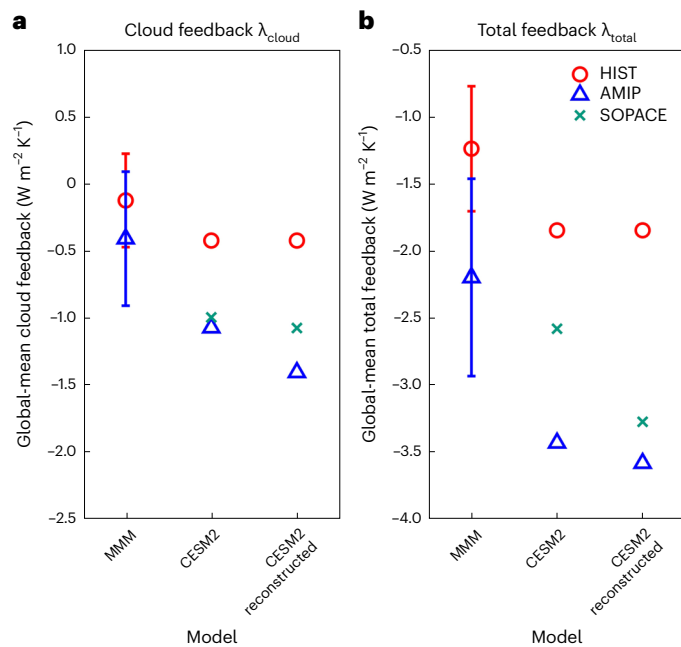
Fig. 5 | Reconstruction of global-mean climate feedbacks via a Green's function. a, Global-mean cloud feedback λ_{cloud} in the historical (HIST; red circles) and AMIP (blue triangles) simulations for the MMM of nine CMIP6 models, with error bars indicating one standard deviation. The same for CESM2, including SOPACE (green crosses). The reconstructed CESM2 feedback is estimated by adding the λ_{cloud} differences from HIST in SOPACE and AMIP, respectively, obtained from the Green's function (that is, global sum of Fig. 4a,b) to HIST (CESM2 reconstructed). **b**, Similar to **a** but for total climate feedback λ_{total} and using Fig. 4c,d for the reconstructed CESM2 estimates. Note that the y-axis interval is the same between the two panels.

Implications of model error in Southeast Pacific clouds

Moreover, we propose that most climate models underestimate the Southern Ocean-driven pattern effect because the stratocumulus cloud feedback in the Southeast Pacific is commonly too weak[39] (Fig. 2 and Extended Data Figs. 3 and 4) and relatedly the cloud fraction response there is underestimated (Extended Data Fig. 2). We propose that this is why the Southeast Pacific has previously not been identified as an important contribution to the global feedbacks (for example, Fig. 11 of ref. 3) as compared to what is shown by the CESM2 model employed here (Extended Data Fig. 7). In CESM2, the Southeast Pacific cloud fraction response is more realistic than the CMIP6 average, being near the upper end of the climate model distribution (Extended Data Fig. 2). Because CESM2 simulates a change in Southeast Pacific cloud fraction and stratocumulus cloud feedback comparable to observations (Fig. 2 and Extended Data Figs. 2–4), we expect the Southern Ocean-driven pattern effect revealed by the CESM2 SOPACE experiment to be realistic. Our study therefore highlights the need for improving low-cloud parameterizations to properly represent the pattern effect, which ultimately controls the temporal evolution of global climate feedback.

Our findings also have important implications for the future because the Southern Ocean is projected to undergo accelerated warming owing to a gradual weakening of ocean heat uptake[24,41]. The projected surface warming amplification over the Southern Ocean will yield a strong positive cloud feedback in the Southeast Pacific, thus further amplifying the surface heating. Our results suggest that this Southern Ocean-driven pattern effect may be underestimated by models, pointing at the possibility of the equilibrium climate sensitivity being higher than previously proposed. The critical role of the Southern Ocean in modulating global climate feedback points to the importance

of monitoring this still observation-sparse region for improving future projections of climate sensitivity.

Online content

Any methods, additional references, Nature Portfolio reporting summaries, source data, extended data, supplementary information, acknowledgements, peer review information; details of author contributions and competing interests; and statements of data and code availability are available at https://doi.org/10.1038/s41561-023-01256-6.

References

1. Soden, B. J. & Held, I. M. An assessment of climate feedbacks in coupled ocean–atmosphere models. *J. Clim.* **19**, 3354–3360 (2006).
2. Stevens, B., Sherwood, S. C., Bony, S. & Webb, M. J. Prospects for narrowing bounds on Earth's equilibrium climate sensitivity. *Earth's Future* **4**, 512–522 (2016).
3. Dong, Y., Proistosescu, C., Armour, K. C. & Battisti, D. S. Attributing historical and future evolution of radiative feedbacks to regional warming patterns using a Green's function approach: the preeminence of the western pacific. *J. Clim.* **32**, 5471–5491 (2019).
4. Zhou, C., Zelinka, M. D. & Klein, S. A. Analyzing the dependence of global cloud feedback on the spatial pattern of sea surface temperature change with a Green's function approach. *J. Adv. Model. Earth Syst.* **9**, 2174–2189 (2017).
5. Fueglistaler, S. Observational evidence for two modes of coupling between sea surface temperatures, tropospheric temperature profile, and shortwave cloud radiative effect in the tropics. *Geophys. Res. Lett.* **46**, 9890–9898 (2019).
6. Andrews, T. & Webb, M. J. The dependence of global cloud and lapse rate feedbacks on the spatial structure of tropical pacific warming. *J. Clim.* **31**, 641–654 (2018).
7. Andrews, T., Gregory, J. M. & Webb, M. J. The dependence of radiative forcing and feedback on evolving patterns of surface temperature change in climate models. *J. Clim.* **28**, 1630–1648 (2015).
8. Zhou, C., Zelinka, M. D. & Klein, S. A. Impact of decadal cloud variations on the Earth's energy budget. *Nat. Geosci.* **9**, 871–874 (2016).
9. Andrews, T. et al. On the effect of historical SST patterns on radiative feedback. *J. Geophys. Res. Atmos.* https://doi.org/10.1029/2022JD036675 (2022).
10. Andrews, T. et al. Accounting for changing temperature patterns increases historical estimates of climate sensitivity. *Geophys. Res. Lett.* **45**, 8490–8499 (2018).
11. Gregory, J. M., Andrews, T., Ceppi, P., Mauritsen, T. & Webb, M. J. How accurately can the climate sensitivity to CO_2 be estimated from historical climate change? *Clim. Dyn.* **54**, 129–157 (2020).
12. Gregory, J. M. & Andrews, T. Variation in climate sensitivity and feedback parameters during the historical period. *Geophys. Res. Lett.* **43**, 3911–3920 (2016).
13. Wills, R. C. J., Dong, Y., Proistosecu, C., Armour, K. C. & Battisti, D. S. Systematic climate model biases in the large-scale patterns of recent sea-surface temperature and sea-level pressure change. *Geophys. Res. Lett.* **49**, e2022GL100011 (2022).
14. Meehl, G. A., Arblaster, J. M., Bitz, C. M., Chung, C. T. Y. & Teng, H. Antarctic sea-ice expansion between 2000 and 2014 driven by tropical Pacific decadal climate variability. *Nat. Geosci.* **9**, 590–595 (2016).
15. Chung, E.-S. et al. Antarctic sea-ice expansion and Southern Ocean cooling linked to tropical variability. *Nat. Clim. Change* https://doi.org/10.1038/s41558-022-01339-z (2022).
16. Zhang, L., Delworth, T. L., Cooke, W. & Yang, X. Natural variability of Southern Ocean convection as a driver of observed climate trends. *Nat. Clim. Change* **9**, 59–65 (2019).

17. Bronselaer, B. et al. Change in future climate due to Antarctic meltwater. *Nature* **564**, 53–58 (2018).

18. Pauling, A. G., Bitz, C. M., Smith, I. J. & Langhorne, P. J. The response of the Southern Ocean and Antarctic sea ice to freshwater from ice shelves in an earth system model. *J. Clim.* **29**, 1655–1672 (2016).

19. Purich, A., England, M. H., Cai, W., Sullivan, A. & Durack, P. J. Impacts of broad-scale surface freshening of the southern ocean in a coupled climate model. *J. Clim.* **31**, 2613–2632 (2018).

20. Polvani, L. M., Waugh, D. W., Correa, G. J. P. & Son, S.-W. Stratospheric ozone depletion: the main driver of twentieth-century atmospheric circulation changes in the Southern Hemisphere. *J. Clim.* **24**, 795–812 (2011).

21. Kostov, Y., Ferreira, D., Armour, K. C. & Marshall, J. Contributions of greenhouse gas forcing and the southern annular mode to historical southern ocean surface temperature trends. *Geophys. Res. Lett.* **45**, 1086–1097 (2018).

22. Hwang, Y.-T., Xie, S.-P., Deser, C. & Kang, S. M. Connecting tropical climate change with Southern Ocean heat uptake. *Geophys. Res. Lett.* **44**, 9449–9457 (2017).

23. Kang, S. M. et al. Walker circulation response to extratropical radiative forcing. *Sci. Adv.* **6**, eabd3021 (2020).

24. Lin, Y.-J., Hwang, Y.-T., Lu, J., Liu, F. & Rose, B. E. J. The dominant contribution of Southern Ocean heat uptake to time-evolving radiative feedback in CESM. *Geophys. Res. Lett.* **48**, e2021GL093302 (2021).

25. Kim, H., Kang, S. M., Kay, J. E. & Xie, S.-P. Subtropical clouds key to Southern Ocean teleconnections to the tropical Pacific. *Proc. Natl Acad. Sci. USA* **119**, e2200514119 (2022).

26. Hartmann, D. L. The Antarctic ozone hole and the pattern effect on climate sensitivity. *Proc. Natl Acad. Sci. USA* **119**, e2207889119 (2022).

27. Ceppi, P. & Gregory, J. M. Relationship of tropospheric stability to climate sensitivity and Earth's observed radiation budget. *Proc. Natl Acad. Sci. USA* **114**, 13126–13131 (2017).

28. Bloch-Johnson, J., Rugenstein, M. & Abbot, D. S. Spatial radiative feedbacks from internal variability using multiple regression. *J. Clim.* **33**, 4121–4140 (2020).

29. Senior, C. A. & Mitchell, J. F. B. The time-dependence of climate sensitivity. *Geophys. Res. Lett.* **27**, 2685–2688 (2000).

30. Rose, B. E. J., Armour, K. C., Battisti, D. S., Feldl, N. & Koll, D. D. B. The dependence of transient climate sensitivity and radiative feedbacks on the spatial pattern of ocean heat uptake. *Geophys. Res. Lett.* **41**, 1071–1078 (2014).

31. Rugenstein, M. A. A., Caldeira, K. & Knutti, R. Dependence of global radiative feedbacks on evolving patterns of surface heat fluxes. *Geophys. Res. Lett.* **43**, 9877–9885 (2016).

32. Danabasoglu, G. et al. The community earth system model version 2 (CESM2). *J. Adv. Model. Earth Syst.* **12**, e2019MS001916 (2020).

33. Zhang, X., Deser, C. & Sun, L. Is there a tropical response to recent observed Southern Ocean cooling? *Geophys. Res. Lett.* **48**, e2020GL091235 (2021).

34. Wood, R. & Bretherton, C. S. On the relationship between stratiform low cloud cover and lower-tropospheric stability. *J. Clim.* **19**, 6425–6432 (2006).

35. Sobel, A. H., Nilsson, J. & Polvani, L. M. The weak temperature gradient approximation and balanced tropical moisture waves. *J. Atmos. Sci.* **58**, 3650–3665 (2001).

36. Shin, Y. et al. Evolution of the tropical response to periodic extratropical thermal forcing. *J. Clim.* **34**, 6335–6353 (2021).

37. Hwang, Y.-T. et al. Relative roles of energy and momentum fluxes in the tropical response to extratropical thermal forcing. *J. Clim.* **34**, 3771–3786 (2021).

38. Newman, M. et al. The Pacific Decadal Oscillation, revisited. *J. Clim.* **29**, 4399–4427 (2016).

39. Myers, T. A. et al. Observational constraints on low cloud feedback reduce uncertainty of climate sensitivity. *Nat. Clim. Change* **11**, 501–507 (2021).

40. Ceppi, P. & Nowack, P. Observational evidence that cloud feedback amplifies global warming. *Proc. Natl Acad. Sci. USA* **118**, e2026290118 (2021).

41. Shi, J.-R., Xie, S.-P. & Talley, L. D. Evolving relative importance of the Southern Ocean and North Atlantic in anthropogenic ocean heat uptake. *J. Clim.* **31**, 7459–7479 (2018).

Methods

Sensitivity to model physics

Here we propose that the recent Southern Ocean cooling might have contributed to anomalously negative climate feedback via remote cloud changes in the Southeast Pacific. If true, the hypothesis implies that inter-model differences in Southeast Pacific cloud feedback should lead to different global feedback changes in response to a given Southern Ocean forcing. To test this, we analyse the multi-model Extratropical–Tropical Interaction Model Intercomparison Project (ETIN-MIP) experiment[42], in which the insolation is reduced over the southern high latitudes (45° S–65° S) in eight independent global coupled climate models. The same data were used in ref. 25, where the magnitude of the remote cooling over the southeastern tropical Pacific was shown to depend on the Southeast Pacific cloud feedback strength. Here we examine if the Southeast Pacific cloud feedback strength also modulates the global climate feedback.

Following ref. 25, we calculate the Southeast Pacific cloud feedback (x axis of Extended Data Fig. 5) by regressing monthly cloud radiative effects in the pre-industrial control simulations onto local SST, using deseasonalized anomalies over 100 years. Although this measure of local Southeast Pacific cloud feedback is different from that used elsewhere in the paper, which is based on global surface temperature, the two metrics are closely related (Extended Data Fig. 5d). The global climate feedbacks (y axis of Extended Data Fig. 5a–c) are computed using the last and the first 20-year average differences of the 150-year integrations, that is, $\lambda = \Delta X/\Delta T$ where Δ indicates the average difference between years 131–150 and 1–20, T is the global-mean surface air temperature. When calculating the total climate feedback λ_{total}, X is the global-mean net top-of-atmosphere radiation; for the shortwave cloud radiative feedback λ_{swcld} over the Southeast Pacific, we take X as the shortwave cloud radiative effect averaged over the trapezoidal area in Fig. 3. We find that the models with a more positive Southeast Pacific cloud feedback tend to show a less negative global climate feedback (Extended Data Fig. 5a), primarily due to the cloud component (Extended Data Fig. 5b). This inter-model relationship confirms that the local Southeast Pacific cloud feedback modulates the global radiative feedback in response to southern extratropical cooling.

At face value, the relationships in Extended Data Fig. 5a,b seem opposite to the argument in our study that a more positive Southeast Pacific cloud feedback causes a more *negative* global feedback. This difference is because contrary to the ETIN-MIP case, in the historical period Southern Ocean cooling occurred in conjunction with global warming. Thus to present our results in a manner comparable with our main findings, we construct a synthetic experiment qualitatively similar to SOPACE, with Southern Ocean cooling superimposed onto global CO_2-driven warming, which we name 4×CO2-SO. We achieve this by adding the ETIN-MIP response to the abrupt 4×CO2 response, using the five models providing data for both experiments. The synthetic 4×CO2-SO experiment is constructed without any weighting, as we are not concerned about the exact magnitude of the feedback differences but are only interested in the inter-model relationship. The difference between 4×CO2-SO and 4×CO2 is then akin to the comparison between SOPACE and HIST in the main manuscript. Although the sample size is limited, Extended Data Fig. 5c clearly indicates that the models with a more positive local λ_{swcld} in the Southeast Pacific show a more negative global climate feedback in 4×CO2-SO relative to 4×CO2-only forcing.

Combined with the finding that CESM2 agrees with observations in simulating a strong Southeast Pacific cloud feedback (Fig. 2 and Extended Data Fig. 3), the results in Extended Data Fig. 5 support our argument that the linkage between Southern Ocean cooling and anomalous negative global feedback simulated by CESM2 is realistic.

Model experiments

We analyse the 90-member historical (HIST) and ten-member AMIP simulations of CESM2 with the Community Atmosphere Model version 6 (ref. 32) with nominal 1° horizontal resolution, which

participated in the CMIP6 (ref. 43). To isolate the effect of Southern Ocean changes, we conduct a 21-member ensemble of the SOPACE experiment[33] with the same CESM2 model. Extended Data Table 1 summarizes the list of CESM2 experiments. SOPACE is forced by the historical radiative forcing of CMIP6 from 1975 to 2014, while restoring SST anomalies at each grid box poleward of 40° S, with a linearly tapering buffer zone between 35° S–40° S, to the observed evolution of SST anomalies taken from the National Oceanic and Atmospheric Administration Extended Reconstruction Sea Surface Temperature v5 (ERSSTv5) dataset[44]. In regions of climatological sea ice cover, SST is restored to the melting temperature of −1.8 °C. The restoring time scale is two days for the 10 m-deep ocean mixed layer. The close agreement of Southern Ocean SST trends between SOPACE and ERSSTv5 (Extended Data Fig. 1b,d) confirms that our experiment design constrains the Southern Ocean SST as intended. Eight SOPACE members are initialized from different members of CESM2-LE[45], a large ensemble suite conducted with CESM2, on 1 January 1975, while other members are initialized from the first member of CESM2-LE on 1 January 1975 with a random initial atmospheric temperature perturbation. The Southern Ocean between 40° S and 60° S cools by 0.08 K over the 35-year period between 1979 and 2013 in SOPACE, while the region warms by 0.37 K in HIST (Extended Data Fig. 1). We choose to analyse the period 1979–2013 when the observed Southern Ocean cooling trend is most prominent. This choice is also constrained by the available data, as CMIP6 AMIP and HIST end in 2014.

Note that the difference in Southern Ocean SST trends between SOPACE and AMIP arises primarily due to different SST observational datasets employed to force the models: ERSSTv5 in the former and Hadley-OI[46] in the latter (Extended Data Fig. 1). Nudging the SSTs over the Southern Ocean causes more heat flux into the ocean, but the realism of this cannot be evaluated due to the lack of significance of observed changes (not shown). While pacemaker-type experiments violate energy conservation, this is an issue common to all experiments with prescribed SST (for example, AMIP). From an energy budget perspective, restoring the Southern Ocean SST does not severely distort the energy balance but causes an anomalous downward top-of-atmosphere flux of ~0.5 W m^{-2} (not shown).

One might question the validity of our results if the Southern Ocean cooling is driven by the Interdecadal Pacific Oscillation-like tropical changes. Indeed, a drawback of pacemaker-type simulations is that regional SST anomalies are restored to observations regardless of the driver. However, we emphasize that even if the Southern Ocean cooling is driven by the tropics, this cooling will still feed back on the tropical SST. In other words, the teleconnection from Southern Ocean to the tropics exists whether the Southern Ocean cooling is locally or remotely driven.

Observational estimate of shortwave low-cloud feedback

The observational and model estimates of shortwave low-cloud feedback in Fig. 2 and Extended Data Figs. 3 and 4 are obtained following the cloud-controlling factor analysis method of ref. 40. While that study considered the aggregated effect of all cloud types, here we focus on the radiative effect of low clouds as in ref. 39. The cloud-controlling factor analysis framework approximates the shortwave low-cloud radiative feedback at each grid point r, $dC_{\text{swcld,low}}(r)/d\bar{T}$ (where $\bar{T}$ denotes global-mean surface temperature), as a sum of components due to local changes in six cloud-controlling factors: SST, EIS, 700 hPa relative humidity (RH_{700}), 700 hPa vertical velocity (ω_{700}), SST advection by the near-surface wind (SSTadv) and near-surface wind speed (WS):

$$\lambda_{\text{swcld,low}}(r) \equiv \frac{dC_{\text{swcld,low}}(r)}{d\bar{T}}$$

$$\approx \frac{\partial C_{\text{swcld,low}}(r)}{\partial \text{SST}(r)}\frac{d\text{SST}(r)}{d\bar{T}} + \frac{\partial C_{\text{swcld,low}}(r)}{\partial \text{EIS}(r)}\frac{d\text{EIS}(r)}{d\bar{T}} + \frac{\partial C_{\text{swcld,low}}(r)}{\partial \text{RH}_{700}(r)}\frac{d\text{RH}_{700}(r)}{d\bar{T}}$$

$$+ \frac{\partial C_{\text{swcld,low}}(r)}{\partial \omega_{700}(r)}\frac{d\omega_{700}(r)}{d\bar{T}} + \frac{\partial C_{\text{swcld,low}}(r)}{\partial \text{SSTadv}(r)}\frac{d\text{SSTadv}(r)}{d\bar{T}} + \frac{\partial C_{\text{swcld,low}}(r)}{\partial \text{WS}(r)}\frac{d\text{WS}(r)}{d\bar{T}}$$

(see ref. 39 for details on the definition of these variables).

Estimating the low-cloud feedback $dC_{\text{swcld,low}}/d\bar{T}$ involves three steps: (1) calculating the monthly low-cloud-induced radiative anomalies, $dC_{\text{swcld, low}}$; (2) calculating the cloud radiative sensitivities of $dC_{\text{swcld, low}}$ onto the controlling factors X, $dC_{\text{swcld, low}}/dX$; (3) multiplying the sensitivities $dC_{\text{swcld, low}}/dX$ by the projected changes in controlling factors, $dX/d\bar{T}$. We describe these three steps in turn below:

(1) For observations, $dC_{\text{swcld, low}}$ is calculated by convolving Moderate Resolution Imaging Spectroradiometer (MODIS) cloud fraction data[47], binned by cloud top pressure and optical depth, with a cloud radiative kernel[48]. Following previous work, we aggregate data from the lowermost two cloud top pressure bins in our calculation of $dC_{\text{swcld, low}}$. We use 20 years of MODIS observations from July 2002 to June 2022. For climate models, we proceed in the same way as for MODIS observations but using historical monthly satellite simulator data for 1981–2000. Apart from CESM2, we use an additional ten CMIP6 models that provide the necessary satellite simulator output to calculate the low-cloud radiative anomalies. All observational and model data is remapped onto a common 5° × 5° grid before further analysis.

(2) The cloud radiative sensitivities, that is, the partial derivatives $\partial C_{\text{swcld, low}}/\partial X$ (where X denotes one of the six controlling factors), are calculated by ridge regression of $\partial C_{\text{swcld, low}}$ onto the controlling factor anomalies ∂X at each grid point r[40]. For observations, the controlling factors are taken from monthly 5th generation European Centre for Medium-Range Weather Forecasts reanalysis (ERA5) data[49]. For all variables, we subtract the monthly-mean climatology before analysis. As predictors, we use controlling factor data from a 25° × 25° domain (that is, 5 × 5 = 25 grid points) centred on the target grid point r. This yields (25 grid points) × (6 controlling factors) = 150 predictors for each regression.

(3) The cloud radiative sensitivities are then multiplied by the changes in controlling factors $dX/d\bar{T}$ taken from the AMIP simulation for the 20-year period 1981–2000, model by model. The changes are calculated by regressing annual-mean values of each controlling factor X, at each grid point r, onto global-mean temperature $\bar{T}$. For observations, we use the CESM2 controlling factor changes, which ensures that the observational estimate is directly comparable to the CESM2 cloud feedback, with any differences solely due to the cloud radiative sensitivities $\partial C_{\text{swcld, low}}/\partial X$ to controlling factors.

Green's functions

The Green's functions in Extended Data Fig. 7 are calculated using the CESM2 amip-piForcing simulation[10,12], where the atmospheric model is forced with observed SSTs and sea ice for the period 1870–2014, while atmospheric composition is kept at pre-industrial levels. Given the absence of forcing, radiative budget variations in this experiment are primarily due to the radiative response to SST changes. The calculation is performed as follows:

• Using annual-mean data, we first decompose the SST anomalies into a component associated with global-mean warming or cooling, SST_{mean}, and the deviation there from $\text{SST}_{\text{pattern}}$. For each annual time step t, we calculate SST_{mean} as the globally averaged SST anomaly relative to the 1870–1879 reference period and subtract this from local SST at each grid point r to obtain the pattern of SST anomalies relative to the global mean:

$$\text{SST}_{\text{pattern}}(r,t) = \text{SST}(r,t) - \text{SST}_{\text{mean}}(t).$$

• We next calculate the corresponding global-mean cloud radiative and total radiative responses $R_{\text{cloud, mean}}$ and $R_{\text{total, mean}}$ associated with SST_{mean}. To do this, we use the climatological difference in cloud radiative effect and net top-of-atmosphere radiative

budget between the amip and amip-p4K experiments, which are identical except for a uniform 4 K difference in SST. These responses to 4 K warming, which we denote $dR_{\text{cloud, 4K}}$ and $dR_{\text{total, 4K}}$, are rescaled according to the time evolution of SST_{mean}:

$$R_{\text{cloud,mean}}(t) = dR_{\text{cloud,4K}} \times \text{SST}_{\text{mean}}(t)/4,$$

$$R_{\text{total,mean}}(t) = dR_{\text{total,4K}} \times \text{SST}_{\text{mean}}(t)/4.$$

• We then obtain the global-mean radiative responses to the amip-piForcing time-evolving SST pattern, $R_{\text{cloud, pattern}}$ and $R_{\text{total, pattern}}$, by subtracting the components due to uniform warming:

$$R_{\text{cloud,pattern}}(t) = R_{\text{cloud}}(t) - R_{\text{cloud,mean}}(t),$$

$$R_{\text{total,pattern}}(t) = R_{\text{total}}(t) - R_{\text{total,mean}}(t).$$

• Finally, we obtain the cloud and total radiative Green's functions as the regression coefficients of $R_{\text{cloud, pattern}}(t)$ and $R_{\text{total, pattern}}(t)$ onto $\text{SST}_{\text{pattern}}(r,t)$, that is, the time-evolving SST anomalies at each grid point r constitute our set of predictors. Here we use ridge regression[50], a variant of multiple regression that mitigates overfitting by minimizing not only the least-squares error (as in traditional multiple linear regression), but also the size of the regression coefficients themselves. The method was recently successfully employed to predict cloud feedback from observable data in models and observations[40]. We exclude high-latitude SSTs poleward of 60° from the regression, where large anomalies occur at the sea ice edge. The resulting set of regression coefficients can be interpreted as partial derivatives of the global radiative response R with respect to SSTs at each grid point r, $\partial R_{\text{pattern}}/\partial \text{SST}(r)$.

Calculating the Green's functions from CESM2 data, rather than relying on pre-calculated Green's functions from other atmospheric models[3,4], ensures that the Green's functions are reflective of CESM2 physics—particularly the strong low-cloud feedback in subtropical subsidence regions (Fig. 2 and Extended Data Figs. 3 and 4), central to our results. This is visible in Extended Data Fig. 7, where substantial global radiative anomalies are associated with SSTs in the eastern subtropical Pacific in addition to the dominant warm-pool signal found in other atmospheric models[3,4].

Data availability

All observational, reanalysis and climate model datasets used in this study are publicly available. The CESM2 SOPACE data and Green's functions are uploaded in https://zenodo.org/record/8115985. CMIP data were obtained from the UK Center for Environmental Data Analysis portal (https://esgf-index1.ceda.ac.uk/search/cmip6-ceda/). ERA5 data were downloaded from the Copernicus Climate Data Store (https://doi.org/10.24381/cds.f17050d7). MODIS data were obtained from the NASA Earthdata portal (https://doi.org/10.5067/MODIS/MCD-06COSP_M3_MODIS.062). ISCCP data were obtained from the National Center for Atmospheric Research's Research Data Archive (https://doi.org/10.5065/D62J68XR).

References

42. Kang, S. M. et al. Extratropical–tropical interaction model intercomparison project (Etin-Mip): protocol and initial results. *Bull. Am. Meteorol. Soc.* **100**, 2589–2606 (2019).

43. Eyring, V. et al. Overview of the Coupled Model Intercomparison Project Phase 6 (CMIP6) experimental design and organization. *Geosci. Model Dev.* **9**, 1937–1958 (2016).

44. Huang, B. et al. Extended reconstructed sea surface temperature, version 5 (ERSSTv5): upgrades, validations, and intercomparisons. *J. Clim.* **30**, 8179–8205 (2017).

45. Rodgers, K. B. et al. Ubiquity of human-induced changes in climate variability. *Earth Syst. Dyn.* **12**, 1393–1411 (2021).

46. Hurrell, J. W., Hack, J. J., Shea, D., Caron, J. M. & Rosinski, J. A new sea surface temperature and sea ice boundary dataset for the community atmosphere model. *J. Clim.* **21**, 5145–5153 (2008).

47. Pincus, R. et al. Updated observations of clouds by MODIS for global model assessment. *Earth Syst. Sci. Data* **15**, 2483–2497 (2023).

48. Zelinka, M. D., Klein, S. A. & Hartmann, D. L. Computing and partitioning cloud feedbacks using cloud property histograms. Part I: cloud radiative kernels. *J. Clim.* **25**, 3715–3735 (2012).

49. Hersbach, H. et al. Global reanalysis: goodbye ERA-Interim, hello ERA5. *EMCMWF* https://doi.org/10.21957/VF291HEHD7 (2019).

50. Hoerl, A. E. & Kennard, R. W. Ridge regression: biased estimation for nonorthogonal problems. *Technometrics* **12**, 15–67 (1970).

51. Norris, J. R. & Evan, A. T. Empirical removal of artifacts from the ISCCP and PATMOS-x satellite cloud records. *J. Atmos. Ocean. Technol.* **32**, 691–702 (2015).

Author contributions

S.K., P.C. and I.-S.K. developed the idea for this study. P.C. provided the Green's function for CESM2 and radiative feedbacks for observations and the CMIP6 ensemble. Y.Y. performed the SOPACE experiments with CESM2. S.K. and P.C. conducted the data analysis and prepared the paper, with valuable input and feedback from Y.Y. and I.-S.K.

Competing interests

The authors declare no competing interests.

Additional information

Extended data is available for this paper at https://doi.org/10.1038/s41561-023-01256-6.

Supplementary information The online version contains supplementary material available at https://doi.org/10.1038/s41561-023-01256-6.

Correspondence and requests for materials should be addressed to Sarah M. Kang or Paulo Ceppi.

Peer review information *Nature Geoscience* thanks Ayumu Miyamoto, Timothy Myers and the other, anonymous, reviewer(s) for their contribution to the peer review of this work. Primary Handling Editor: Tom Richardson, in collaboration with the *Nature Geoscience* team.

**Reprints and permissions information** is available at www.nature.com/reprints.

a HIST
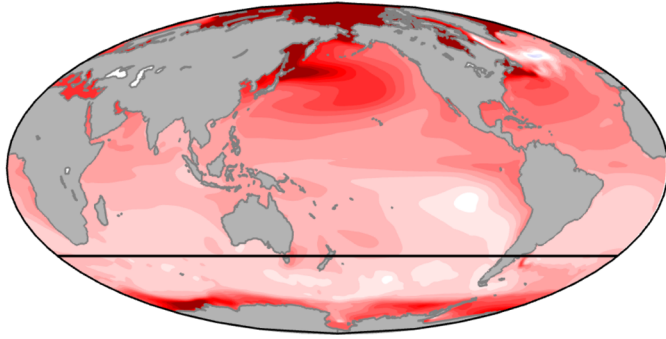
b SOPACE

c AMIP

d ERSSTv5

-2 -1.5 -1 -0.5 0 0.5 1 1.5 2
K/35yr
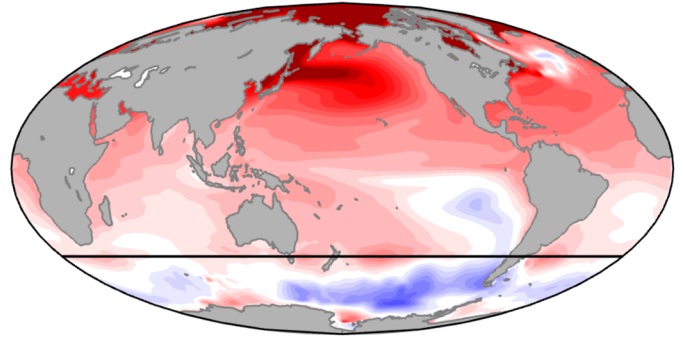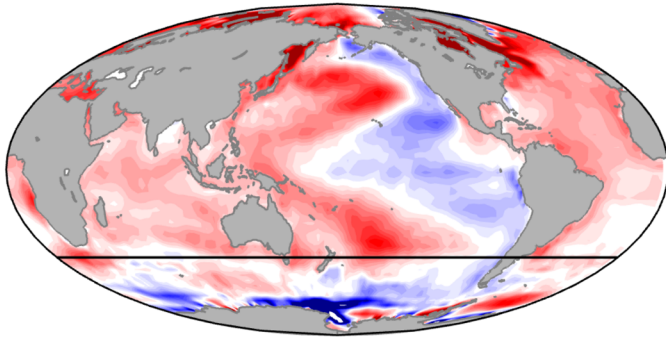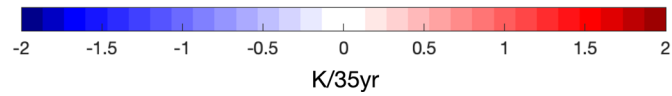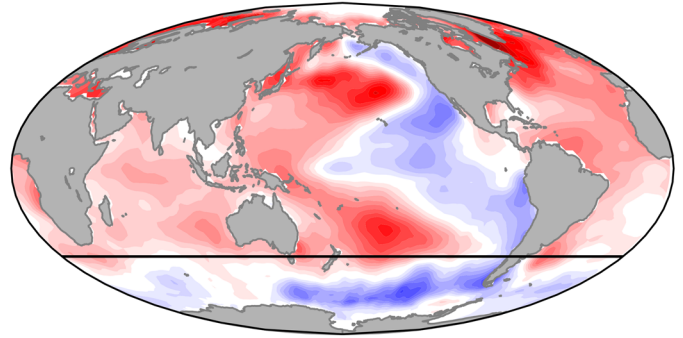
Extended Data Fig. 1 | Linear trends of SST for 1979–2013. a, historical (HIST), **b**, SOPACE, **c**, AMIP experiments, and **d**, ERSSTv5 data[44]. The nudging region is demarcated by a black line.
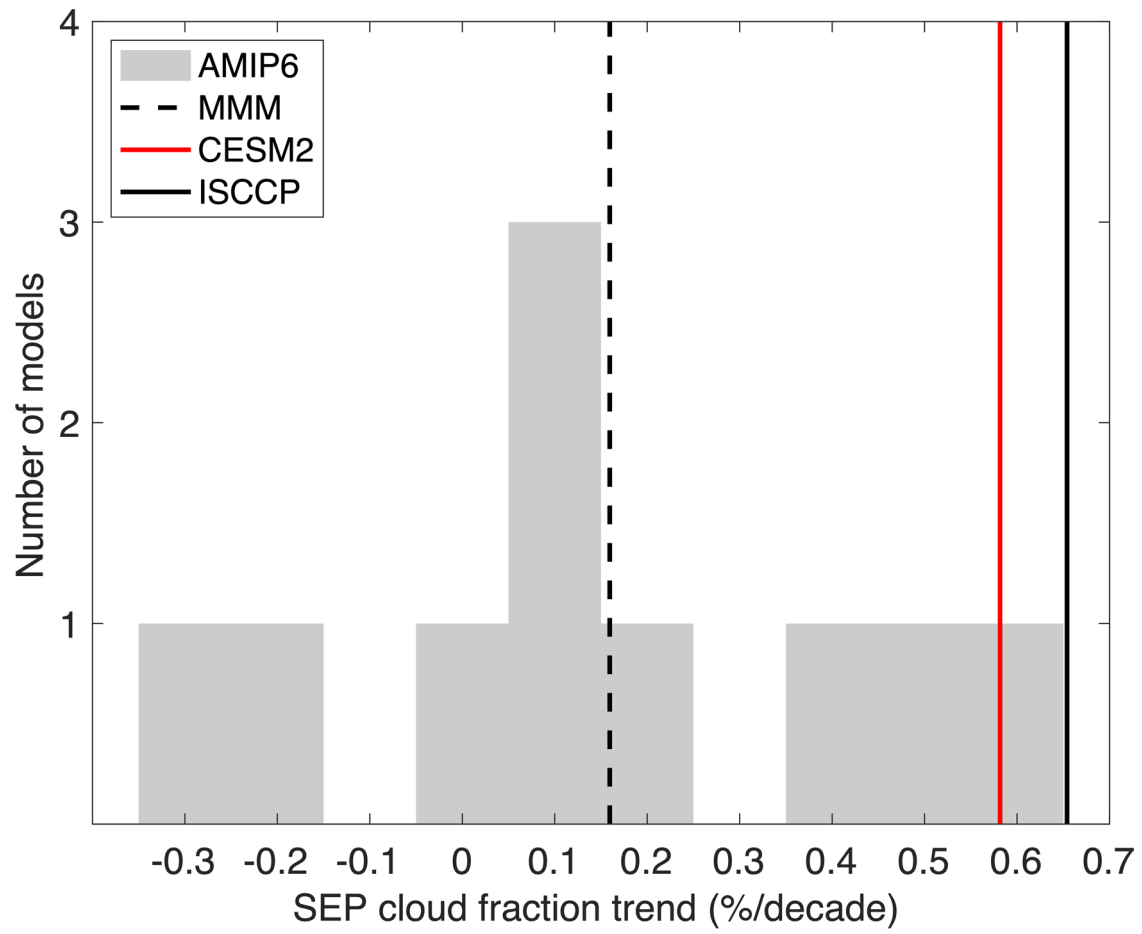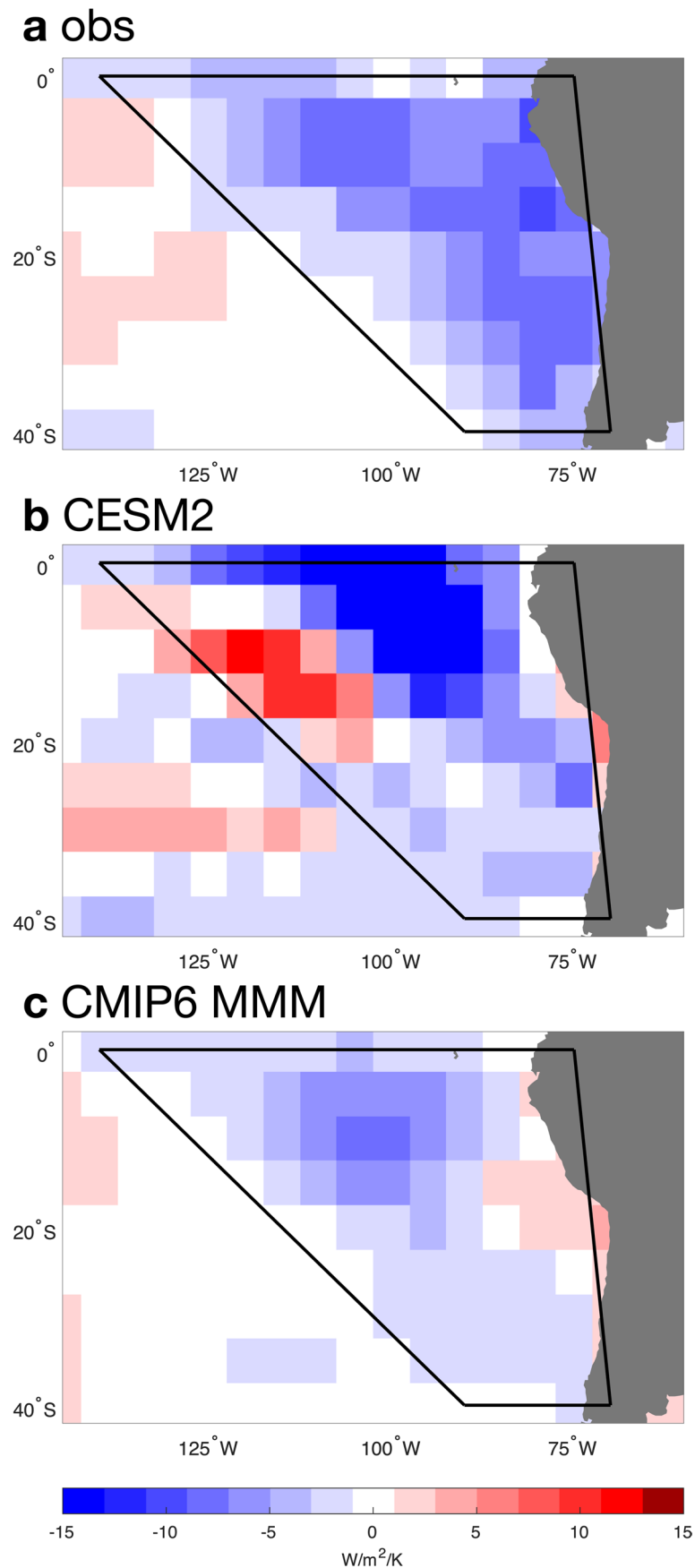
Extended Data Fig. 2 | Southeast Pacific cloud fraction trends. Histogram of linear trends of Southeast Pacific cloud fraction in 11 AMIP6 simulations over 1984–2009, the common period between the ISCCP observations in a black solid line and AMIP6, with the multi-model mean in a black dashed line and the CESM2 AMIP in a red line. We use the corrected ISCCP data provided by Ref. 51, as the raw ISCCP trends mostly show artifacts associated with changes in the observation system, even for the newest dataset ISCCP-H. The global-mean anomalies have been removed in the AMIP6 simulations prior to calculating the trends, for consistency with the processing of the corrected ISCCP trends where global cloud fraction anomalies are set to zero.
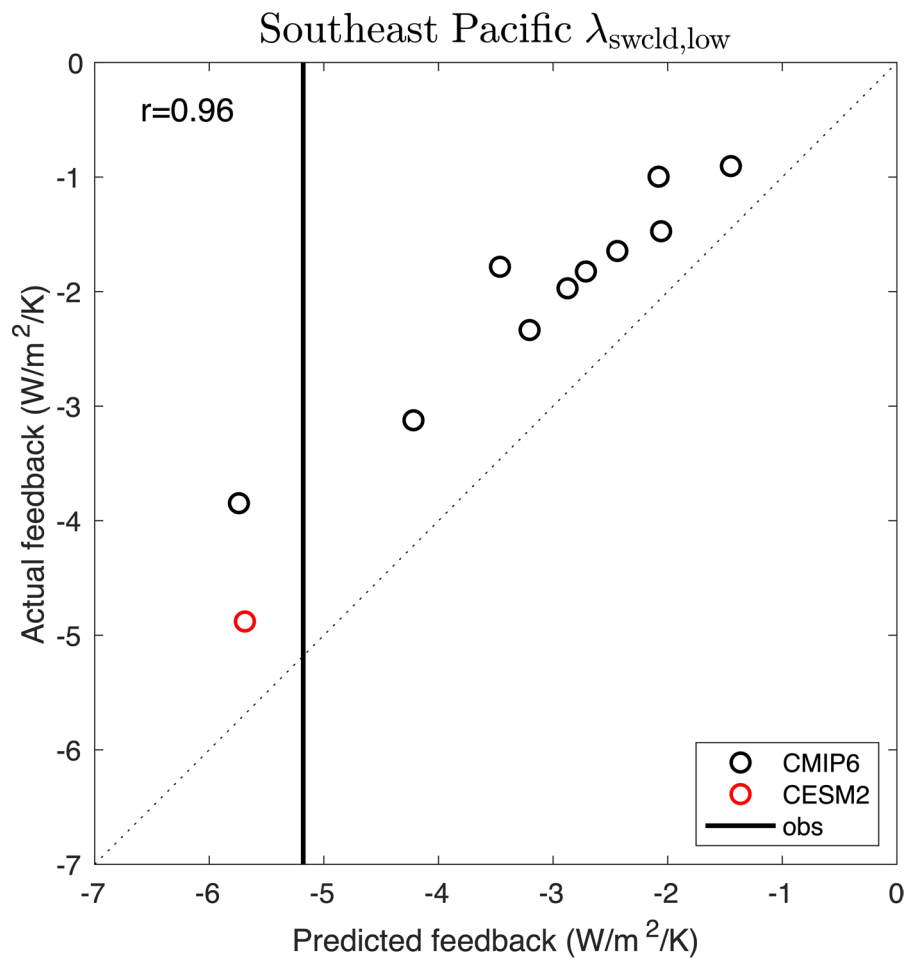
Extended Data Fig. 3 | Southeast Pacific-averaged shortwave low-cloud radiative feedbacks. Scatterplot of Southeast Pacific-averaged shortwave low-cloud radiative feedbacks $\lambda_{swcld,low}$ predicted via cloud controlling factor analysis on the abscissa (see Methods; Fig. 5) versus actual feedbacks on the ordinate (that is, diagnosed from the AMIP experiments by regressing annual-mean, global-mean cloud radiative anomalies onto global-mean surface air temperature $\bar{T}$). Black solid line indicates the observed estimate inferred from MODIS observations and the red circle indicates the CESM2 value. Compared to most other CMIP6 models, CESM2 exhibits a stronger low-cloud shortwave feedback, consistent with observations.
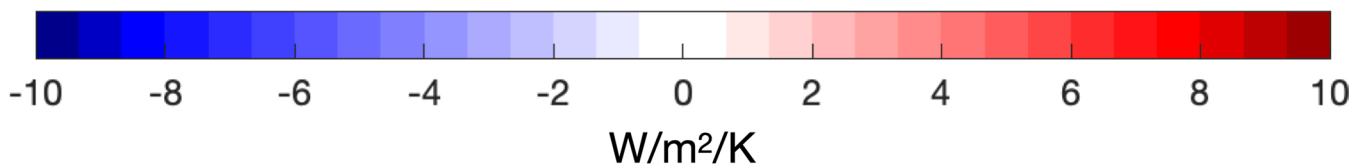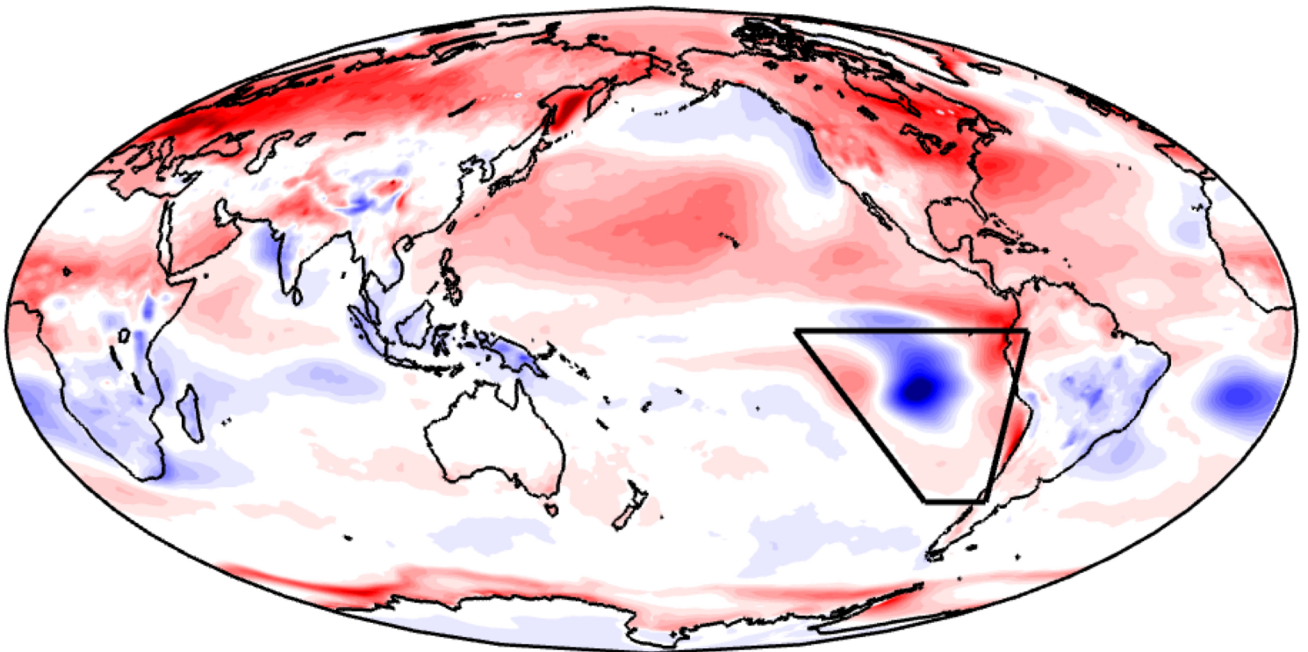
Extended Data Fig. 4 | Spatial distribution of shortwave low-cloud radiative feedbacks. Shortwave low-cloud radiative feedbacks $\lambda_{swcld,\,low}$ in the Southeast Pacific region, predicted from cloud-controlling factor analysis (see Methods), in **a**, MODIS, **b**, CESM2 AMIP experiment, and **c**, AMIP6 experiments from 10 other models than CESM2. Area-averages in the trapezoidal area are compared in Extended Data Fig. 3.
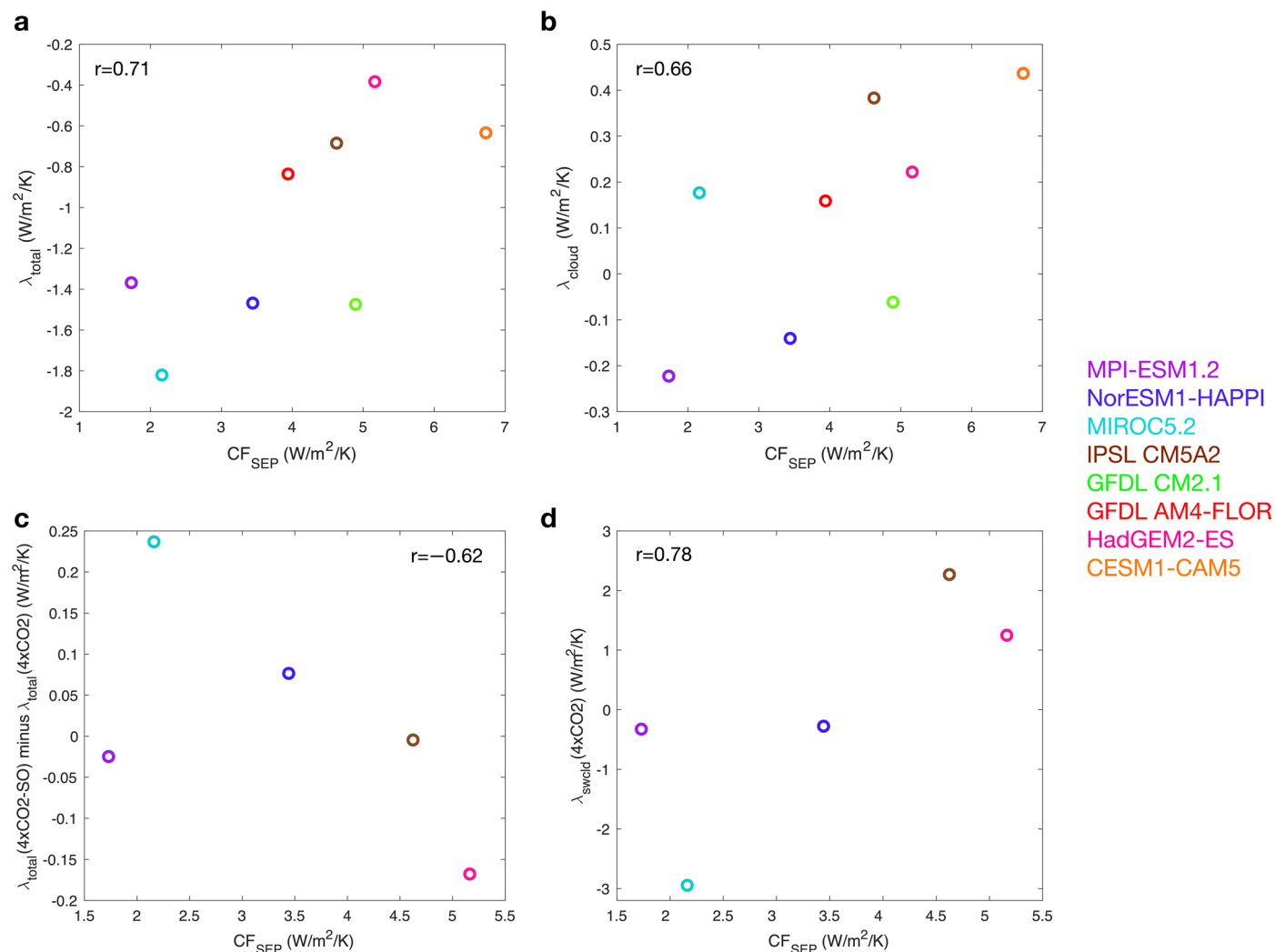
Extended Data Fig. 5 | Inter-model analysis using ETIN-MIP data. Global-mean **a**, total climate feedback λ_{total} and **b**, net cloud feedback λ_{cloud} from the multi-model ETIN-MIP experiments with reduced insolation between 45°S–65°S, versus Southeast Pacific cloud feedback strength estimated from the pre-industrial control run CF_{SEP} (that is, shortwave cloud radiative effect regressed onto local SSTs, with both variables de-trended and deseasonalized). **c**, Global-mean total climate feedback difference between the synthetic experiment 4xCO2-SO and 4xCO2, versus CF_{SEP}. **d**, Comparison of Southeast Pacific cloud feedback metrics based on local temperature (CF_{SEP} in the abscissa) versus global-mean temperature (4xCO2 shortwave cloud feedback in the ordinate, calculated as shortwave cloud radiative effect regressed onto global surface air temperature). The two metrics are closely related with a correlation coefficient of 0.78.

a HIST λ$_{cloud}$
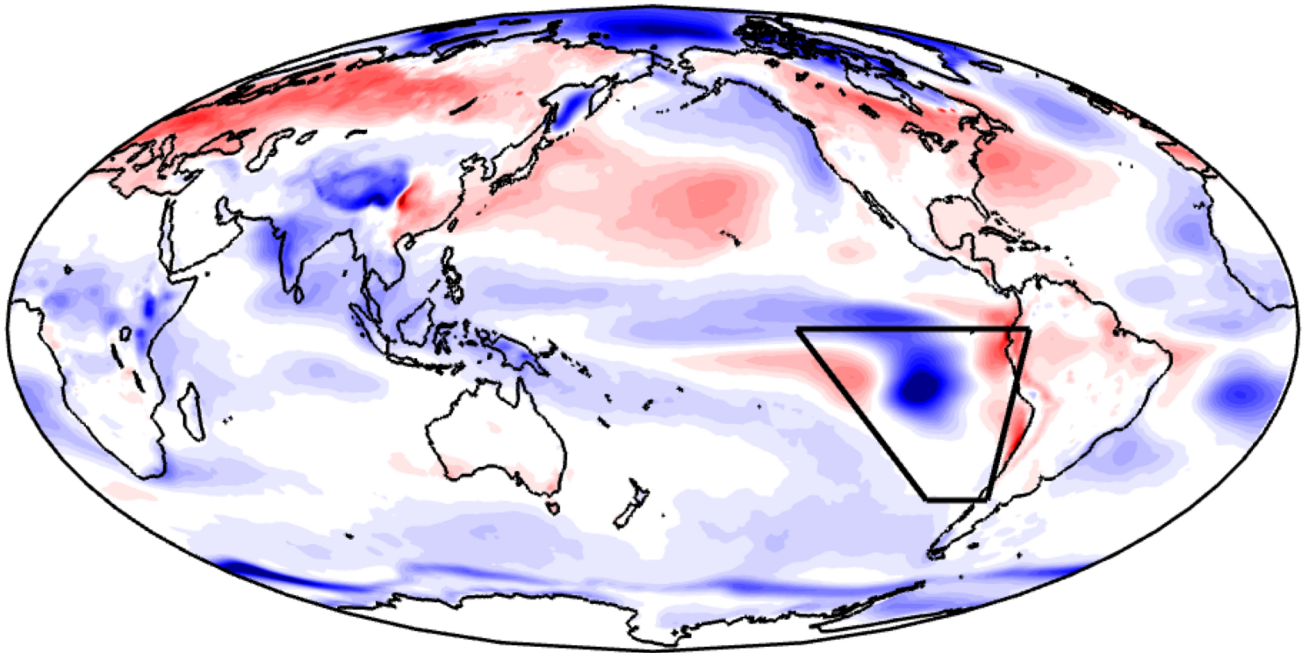
b HIST λ$_{total}$

Extended Data Fig. 6 | Spatial distribution of climate feedbacks. a, Cloud feedback λ_{cloud} and **b**, total climate feedback λ_{total} in HIST.

a GF$_{cloud}$

b GF$_{total}$

W/m²/K

$\times 10^{-3}$
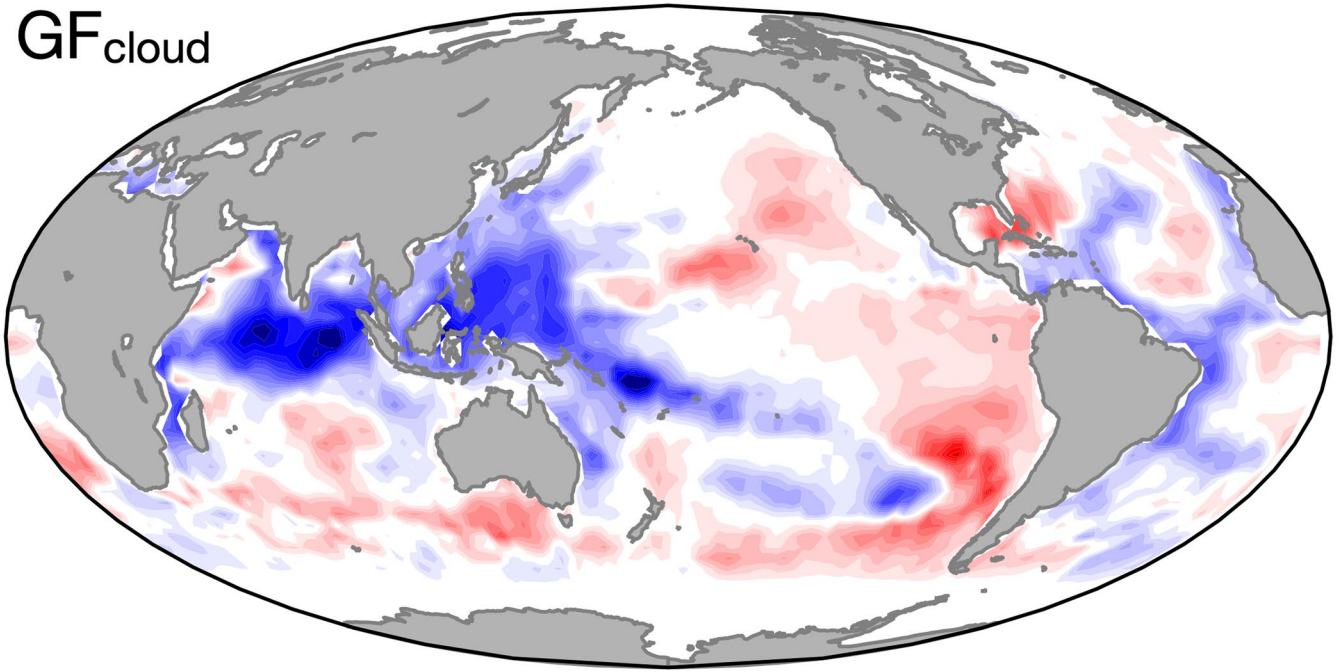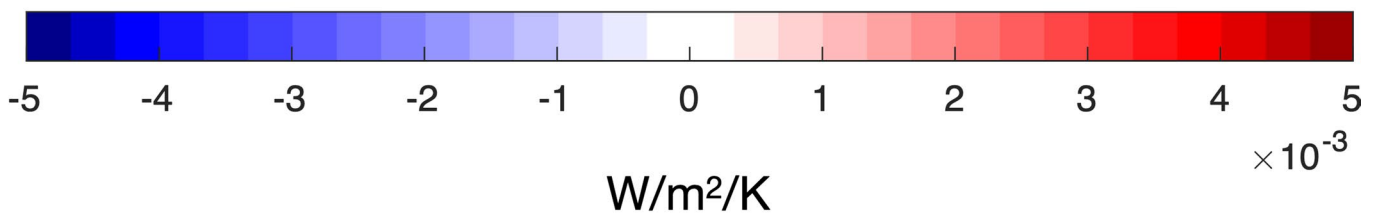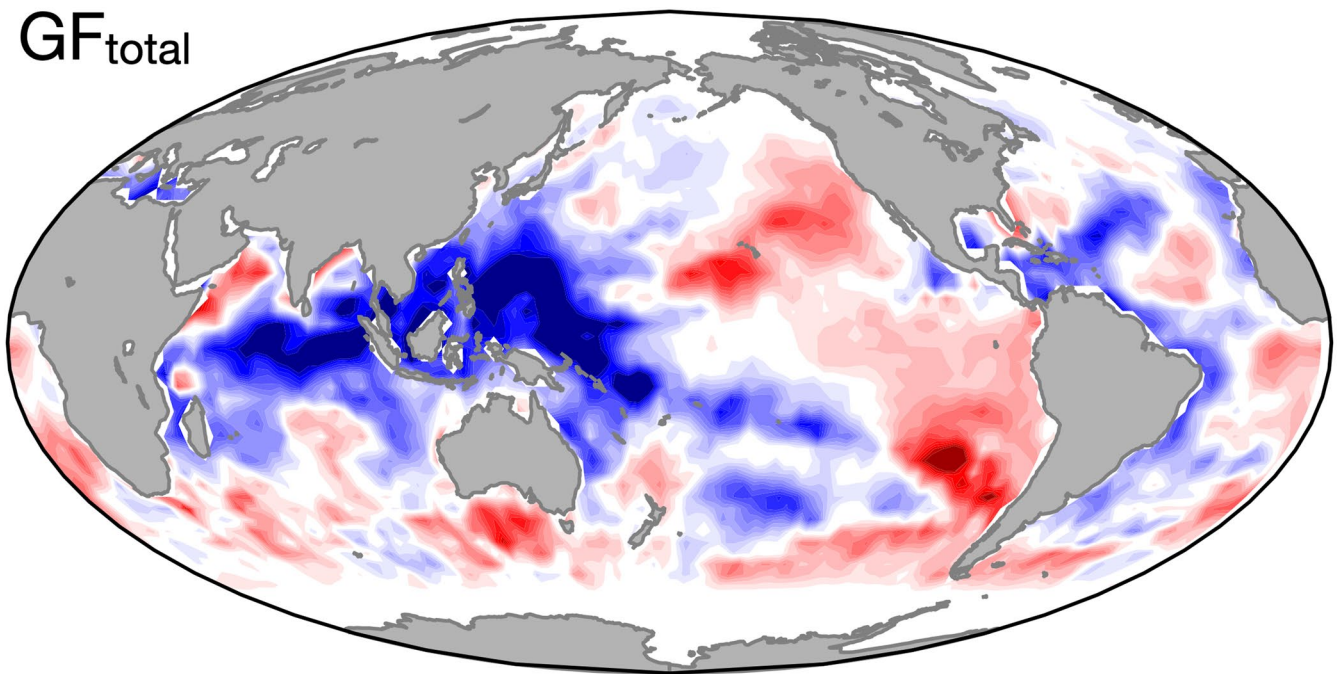
Extended Data Fig. 7 | Green's function from CESM2. a, Global-mean net cloud radiative effect (CRE) changes as a function of local SST changes, corresponding to the Green's function for cloud feedback. **b**, Similar to **a**, but for the net TOA radiation response.

Extended Data Table 1 | List of CESM2 experiments

Experiment name	Experiment description	Ensemble size	Reference
HIST	Large-ensemble coupled simulation of the recent past	90	Rodgers et al. (2021)
AMIP	Observed SSTs and sea-ice prescribed	10	Eyring et al. (2016)
SOPACE	SST anomalies poleward of 40°S restored to observations	21	Zhang et al. (2021)

Experiment description of HIST, AMIP, and SOPACE.